



Electrochromic properties of nanostructured tungsten trioxide (hydrate) films and their applications in a complementary electrochromic device

Zhihui Jiao^a, Jinmin Wang^a, Lin Ke^b, Xuewei Liu^c, Hilmi Volkan Demir^{a,d,e}, Ming Fei Yang^a, Xiao Wei Sun^{a,f,*}

^a School of Electrical and Electronic Engineering, Nanyang Technological University, Nanyang Avenue, Singapore 639798, Singapore

^b Institute of Material Research and Engineering, A*STAR (Agency for Science, Technology and Research), Research Link, Singapore 117602, Singapore

^c School of Physical and Mathematical Sciences, Nanyang Technological University, Nanyang Avenue, Singapore 637371, Singapore

^d Department of Electrical and Electronics Engineering, Department of Physics, UNAM – Institute of Materials Science and Nanotechnology, Bilkent University, Bilkent, Ankara 06800, Turkey

^e School of Physical and Mathematical Sciences, Nanyang Technological University, Nanyang Avenue, Singapore 639798, Singapore

^f Department of Applied Physics, College of Science, and Tianjin Key Laboratory of Low-Dimensional Functional Material Physics and Fabrication Technology, Tianjin University, Tianjin 300072, China

ARTICLE INFO

Article history:

Received 31 August 2011

Received in revised form

16 December 2011

Accepted 18 December 2011

Available online 26 December 2011

Keywords:

Electrochromism

Tungsten trioxide

Thin film

Complementary device

ABSTRACT

Orthorhombic hydrated tungsten trioxide ($3\text{WO}_3 \cdot \text{H}_2\text{O}$) films consisted of nanosticks and nanoparticles were prepared on fluorine doped tin oxide (FTO)-coated substrate by a facile and template-free hydrothermal method using ammonium acetate ($\text{CH}_3\text{COONH}_4$) as the capping agent. Irregular nanobrick films were obtained without capping agent. Due to the highly rough surface, the nanostick/nanoparticle film depicts faster ion intercalation/deintercalation kinetics and a greater coloration efficiency ($45.5 \text{ cm}^2/\text{C}$) than the nanobrick film. A complementary electrochromic device based on the nanostick/nanoparticle $3\text{WO}_3 \cdot \text{H}_2\text{O}$ film and Prussian blue (PB) was assembled. As a result, the complementary device shows a higher optical modulation (54% at 754 nm), a larger coloration efficiency ($151.9 \text{ cm}^2/\text{C}$) and faster switching responses with a bleaching time of 5.7 s and a coloring time of 1.3 s than a single $3\text{WO}_3 \cdot \text{H}_2\text{O}$ layer device, making it attractive for a practical application.

© 2011 Elsevier Ltd. All rights reserved.

1. Introduction

Upon electron-transfer or redox reactions, materials that undergo reversible color changes with variations in their optical spectra are called electrochromic materials [1–3]. Electrochromic devices composed of these materials, which allow for controlling color cycles, have attracted great interest thanks to their applications important for smart windows [4–6], displays [7,8] and antiglare mirrors [9]. The tunable light transmittance resulting from the color change of the electrochromic films is much desired in smart windows, which do not only increase the aesthetics of traditional windows but also save energy by reducing heating or cooling loads of the building interiors [10]. Among various electrochromic materials, tungsten oxide (WO_3) has been extensively studied because of its high coloration efficiency and high cyclic stability compared with other transition metal oxides [11].

Moreover, WO_3 -based electrochromic devices exhibit low power consumption, a good memory effect and a high contrast ratio [12], offering the desired advantages in smart windows and displays. It is widely recognized that nanostructured WO_3 , in comparison to their compact bulk forms, offer potential advantages in electrochromic application due to their large surface area that could both increase the contact area between the electrode and electrolyte and reduce the diffusion path of ions through the porous structures [13]. And the electrochromic efficiency of WO_3 can be further improved by doping suitable metal ions with higher electronegativity or lower oxidizing capability than W ions, such as Mo and Ti [14,15]. Recently, one-dimensional (1D) WO_3 nanostructures with large surface areas, including nanowires [16,17], nanorods [18,19] and nanobelts [20], have been investigated. For electrochromic applications, WO_3 nanostructures need to be assembled as a thin film on conductive substrates and the microstructures of the film concerning the electrochromic performance largely depend on the film assembling techniques and processing conditions. Such thin films of WO_3 have been grown by vacuum deposition [21], electrodeposition [22], sol-gel [23] and hydrothermal method [24,25]. Hydrothermal approach is one of the most promising methods for fabricating WO_3 film because of its merits of low cost, low

* Corresponding author at: School of Electrical and Electronic Engineering, Nanyang Technological University, Nanyang Avenue, Singapore 639798, Singapore. Tel.: +65 67905369; fax: +65 67933318.

E-mail address: exwsun@ntu.edu.sg (X.W. Sun).

reaction temperature, flexible substrate selection and easy scaling-up for production. Moreover, the microstructures of WO_3 films grown by hydrothermal approach can be precisely tailored by varying the precursor concentration, temperature, duration, and adopting various surfactants and capping agents.

To date, a number of hydrothermal methods have been developed for preparing 1D WO_3 nanostructures, including nanorods [19] and nanoribbons [26] by adding different inorganic salts as capping agents. However, previous reports of directly grown WO_3 thin films on substrate using a template-free hydrothermal process and their corresponding electrochromic characteristics have been quite limited. For example, Tu's group reports a hydrothermally grown WO_3 nanowire arrays film recently [27]. A high coloration efficiency of $102.8 \text{ cm}^2/\text{C}$ and fast switching response of 4.2 s for coloration and 7.6 s for bleaching is achieved for this film. Our group has also fabricated nanobrick WO_3 film on transparent conductive substrate using a crystal-seed-assisted hydrothermal method previously [24]. The film shows a good cyclic stability and comparable coloration efficiency ($38.2 \text{ cm}^2/\text{C}$). Although considerable achievements have been made, the electrochromic properties of hydrothermally grown nanostructured WO_3 films can be further improved by increasing their surface area. Moreover, the capping agent effects on the morphology of the hydrothermally grown WO_3 films and their resultant electrochromic characteristics have not been totally understood yet.

Compared with a single layer electrochromic device, it is well known that a complementary device containing two proper electrochromic layers could further improve the performance, such as the optical modulation, cyclic stability and coloration efficiency [28,29]. Prussian blue (PB, iron (III) [hexacyanoferrate (II)]), a coordination-compounded transition metal hexacyanometallate, is a suitable complementary electrochromic material to WO_3 due to its outstanding electrochromic performance and proper operational voltage range. Although complementary electrochromic devices with improved properties based on electrodeposited WO_3 and PB films have been reported [30], to the best of our knowledge, little work has been done on applying the hydrothermally grown nanostructured hydrated tungsten oxide films in such kind of devices.

In this work, we make an attempt to grow nanostructured WO_3 films directly on FTO-coated glass by a hydrothermal method using ammonium acetate ($\text{CH}_3\text{COONH}_4$) as the capping agent. The capping effects of $\text{CH}_3\text{COONH}_4$ on the structure, morphology and electrochromic property of the resulting nanostructured hydrated tungsten oxide films are investigated. Moreover, a complementary electrochromic device combining the hydrated tungsten oxide film with PB film is fabricated and, as a result, increased optical modulation and coloration efficiency is demonstrated.

2. Experimental

2.1. Preparation of crystal seed layers, precursor and hydrothermal treatment

The detailed procedures for preparing crystal seed layers can be found elsewhere [24]. In a typical experiment for preparing the precursor, $\text{Na}_2\text{WO}_4 \cdot 2\text{H}_2\text{O}$ (0.0655 g) was dissolved into 20 mL of de-ionized water and then 4 mL of HCl was added into the solution until no more precipitate was formed. The above suspension was kept in ice bath for about 10 min, then the top liquid part was removed and de-ionized water was added to obtain a 20 mL suspension. Subsequently H_2O_2 (0.2 g) was added into the above suspension under intensely stirring and heating. The white precipitate was dissolved and a transparent solution was obtained. After stirring for 5 min, $\text{CH}_3\text{COONH}_4$ (0.1 g) was added as the capping

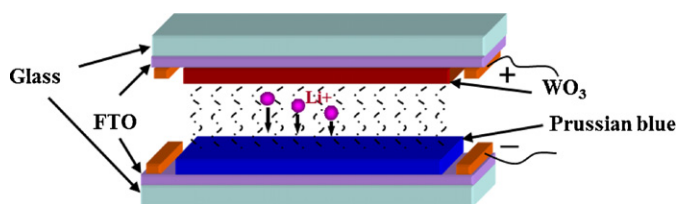


Fig. 1. Schematic of the complementary device.

agent. Then NaOH (1 mol) solution was slowly mixed into this solution while rigorously stirring until the pH value of the solution reached 1.5. For the purpose of comparison, a solution without adding capping agent was also used. The as-prepared solutions were transferred into autoclaves as precursors for hydrothermal treatments. The FTO glasses coated by WO_3 seed layers were put into autoclaves and the hydrothermal process was kept at 180°C for 18 h.

2.2. Electrodeposition of PB and preparation of electrochromic device

The electrodeposition of PB film was carried out by a standard three-electrode system, where a clean FTO served as the working electrode, a platinum sheet as the counter electrode, and a

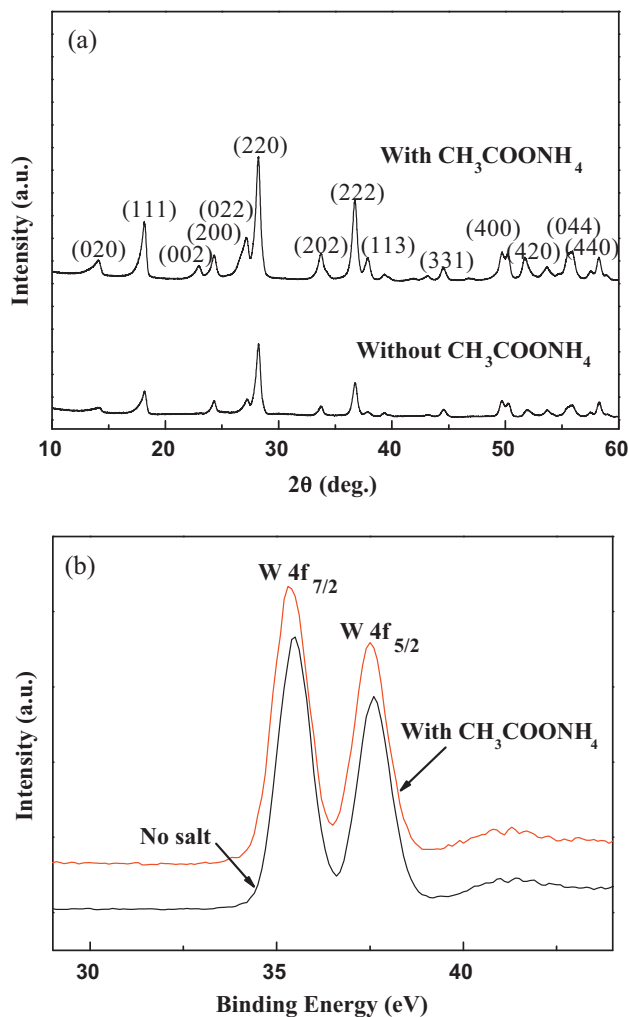


Fig. 2. XRD patterns (a) and (b) tungsten 4f region XPS spectra of the as-synthesized thin films grown with and without $\text{CH}_3\text{COONH}_4$.

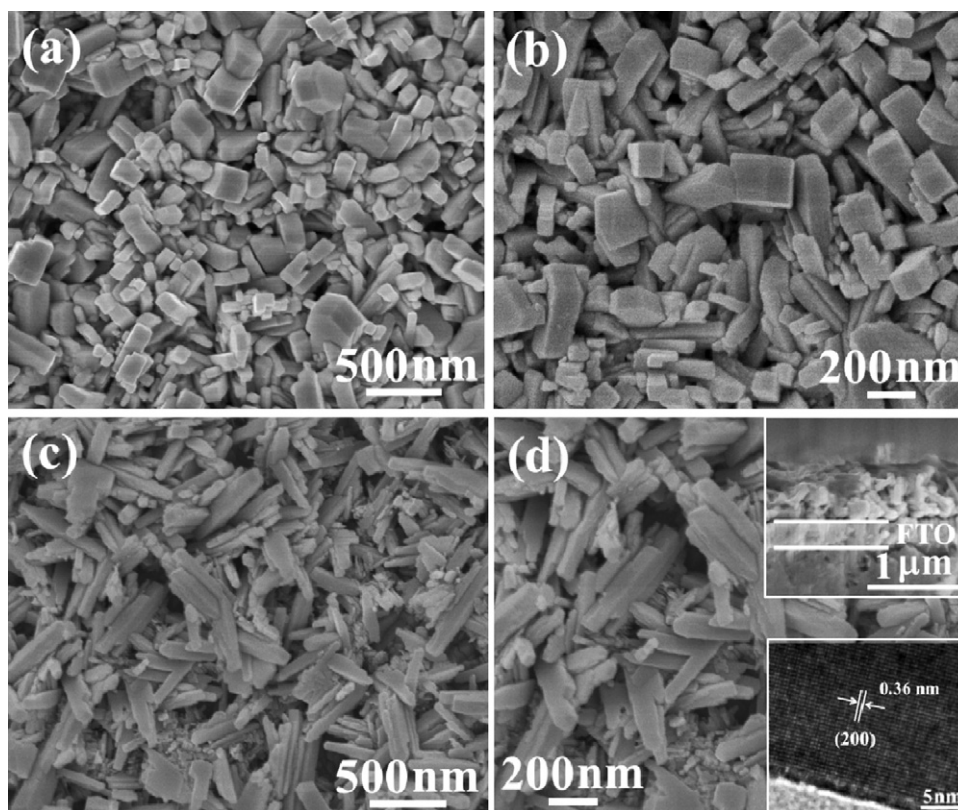


Fig. 3. FESEM images of (a) and (b) the nanobrick $3\text{WO}_3 \cdot \text{H}_2\text{O}$ thin film grown without $\text{CH}_3\text{COONH}_4$; and (c) and (d) nanostick/nanoparticle film with $\text{CH}_3\text{COONH}_4$. Insets: cross-sectional and HRTEM image.

$\text{Ag}/\text{AgCl}/\text{sat'd KCl}$ solution as the reference electrode. The electrodeposition bath of PB contained 10 mmol $\text{K}_3\text{Fe}(\text{CN})_6$, 10 mmol FeCl_3 and 0.1 mol KCl and the electrodeposition of PB thin film was carried out by applying a constant cathodic current density of $50 \mu\text{A}/\text{cm}^2$ for 300 s. The thickness of the as-deposited PB film is about 450 nm (measured by a TENCOR P-10 Surface Profiler). Then the WO_3 working electrode and PB counter electrode were sandwiched together with hot-melt Surlyn spacers. A liquid electrolyte composed of 0.2 mol LiClO_4 in γ -butyrolactone (γ -BL) was introduced between the two electrodes by capillary action. Finally the cell was sealed with epoxy, which is schematically shown in Fig. 1.

2.3. Characterization

The phases of the synthesis products were identified by X-ray powder diffraction (XRD, Siemens), using $\text{Cu K}\alpha_1$ ($\lambda = 0.15406 \text{ nm}$) radiation. X-ray photoelectron spectroscopy (XPS) data were obtained on a Kratos AXIS spectrometer with monochromatic $\text{Al K}\alpha$ (1486.71 eV) X-ray radiation. The morphologies of the as-prepared thin films were observed by field emission scanning

electron microscope (FESEM, JSM 6340). High-resolution transmission electron microscopy (HRTEM) image was obtained by a JEM-2100 microscope using an accelerating voltage of 200 kV. The optical absorbance and transmittance spectra were measured using a UV/V is spectrophotometer (JESCO V670). Electrochemical measurements were performed by a three-electrode system (VersaSTAT 3F Potentiostat/Galvanostat) with LiClO_4 (0.2 mol) in γ -BL as the electrolyte, Pt sheet as the counter electrode and $\text{Ag}/\text{AgCl}/\text{sat'd KCl}$ as the reference electrode.

3. Results and discussion

3.1. Structures and morphologies of as-prepared films

Fig. 2(a) shows the X-ray diffraction (XRD) patterns of the as-prepared thin films grown with and without $\text{CH}_3\text{COONH}_4$. Both films show the same crystalline structure and all peaks can be well indexed to the orthorhombic phase of $3\text{WO}_3 \cdot \text{H}_2\text{O}$ (JCPDF 87-1203) with the corresponding lattice constants of $a = 7.345$, $b = 12.547$ and $c = 7.737 \text{ \AA}$. The sharp peaks indicate the good crystalline quality of

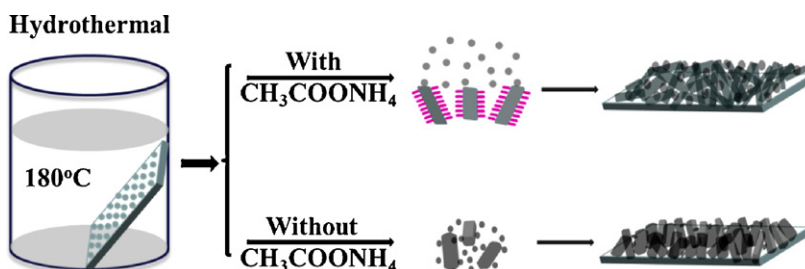


Fig. 4. Schematic illustration of the formation process of the as-grown thin films.

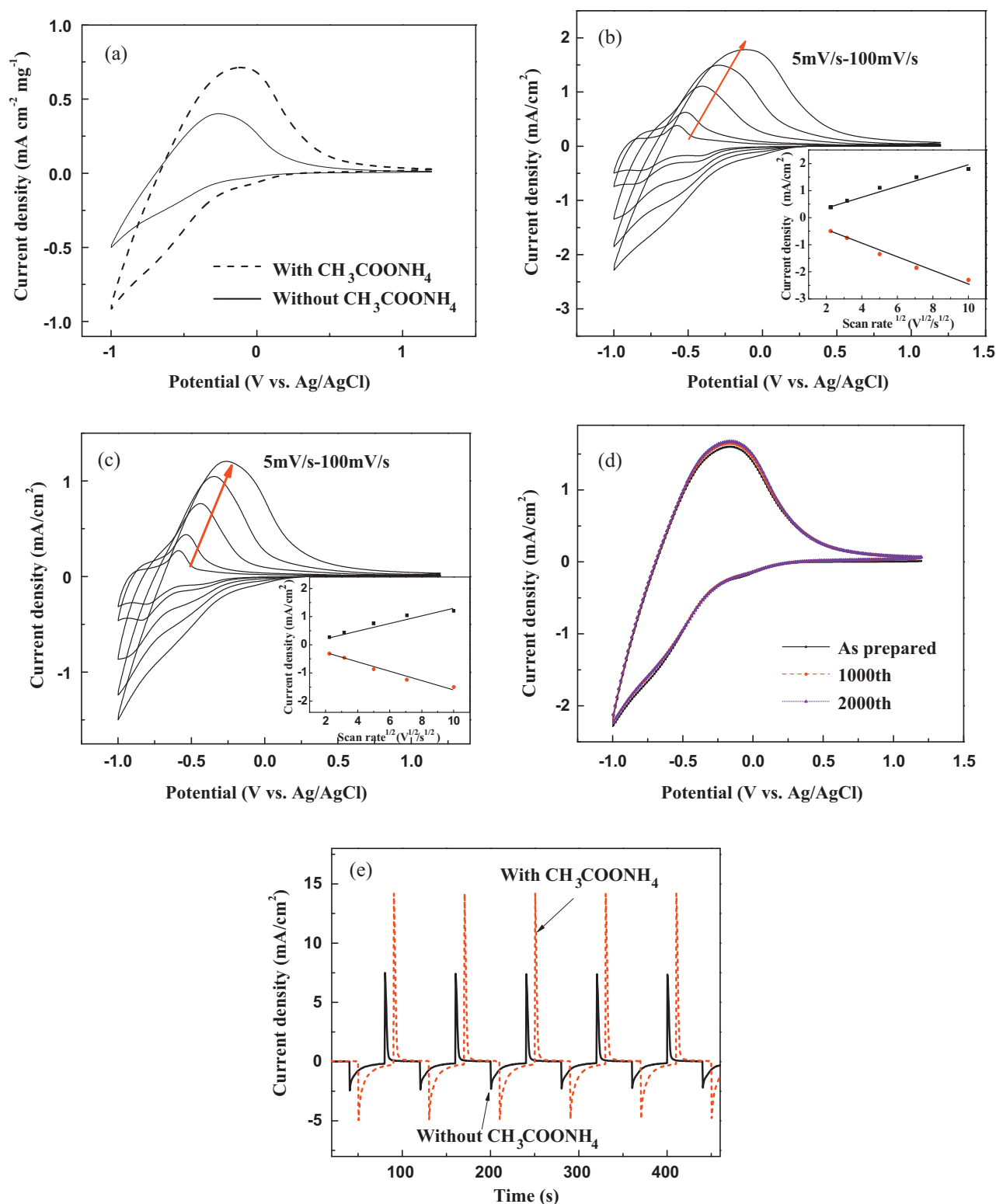


Fig. 5. (a) Cyclic voltammograms (CVs) of the nanostick/nanoparticle and nanobrick 3WO₃·H₂O films in γ-butyrolactone with 0.2 mol LiClO₄; (b) and (c) CVs of the nanostick/nanoparticle and nanobrick film at the scan rates of 5, 10, 25, 50 and 100 mV/s, respectively. Insets: the cathodic/anodic peak current density as a function of the square root of the scan rates; (d) CVs of the nanostick/nanoparticle film after 1st, 1000th, and 2000th cycles; and (e) chronoamperometry (CA) curve of the as-synthesized films recorded at ±0.5 V for 40 s.

the as-fabricated films. The electrochromic performance of WO₃ is closely related to its crystallinity. Crystalline WO₃ has a better stability to endure acidic electrolyte without degradation for a longer cyclic time compared to amorphous one, but at the cost of slower response time and smaller coloration efficiency arising from its

smaller specific surface area [31]. By increasing the porosity and precisely controlling the crystal size, crystalline WO₃ films with good stability and fast response can simultaneously be achieved. Fig. 2(b) shows the X-ray photoelectron spectroscopy (XPS) data of the as-synthesized films. The binding energies of the samples were

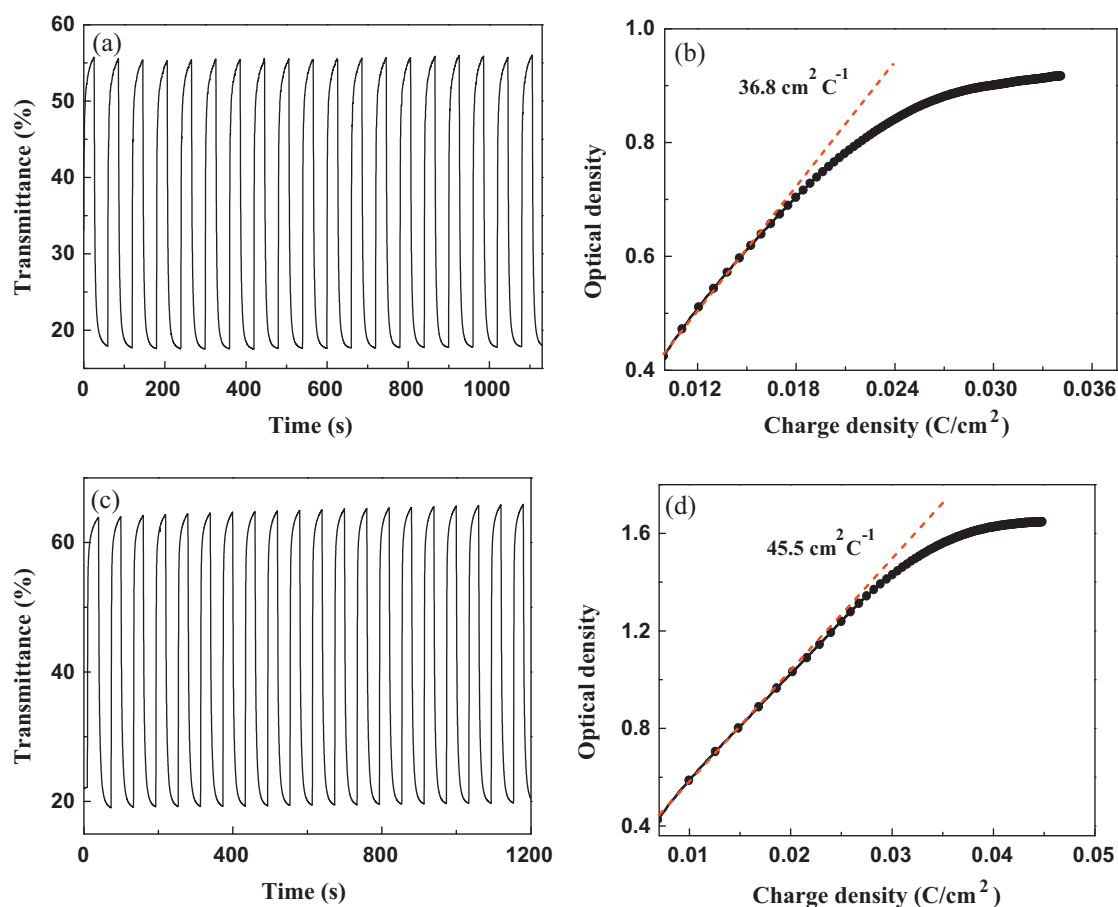


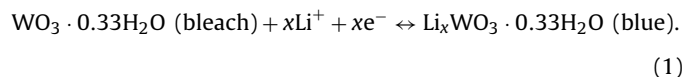
Fig. 6. *In situ* transmittance response and coloration efficiency at 754 nm for the nanobrick film (a and b) and the nanostick/nanoparticle film (c and d).

corrected using a value of 284.5 eV for the C 1s peak of carbon. For both films, two well-resolved peaks at about 35.5 and 37.6 eV in the spectra are attributed to the spin orbit split doublet peaks of W $4f_{7/2}$ and W $4f_{5/2}$, respectively. These two peaks are well separated without any shoulders, indicating that all W atoms are in the +6 oxidation states.

Fig. 3 shows the morphologies of the as-synthesized films. It can be seen that the film grown without $\text{CH}_3\text{COONH}_4$ consists of irregular aggregated nanobricks with sizes ranging from tens to hundreds of nanometers (see Fig. 3(a) and (b)), while thin film made up of stacked nanosticks and nanoparticles is obtained by adding $\text{CH}_3\text{COONH}_4$ as the capping agent (Fig. 3(c) and (d)). The nanosticks with an average length of ~ 50 nm are horizontally stacked together, leading to a coarse surface. A lot of small nanoparticles with sizes of tens of nanometers are accumulated underneath these sticks. Clear lattice fringes of the high-resolution transmission electron microscopy (HRTEM) image from a nanostick (inset of Fig. 3(d)) indicate its single crystalline quality. The inset cross-sectional image shows that the film with a thickness of ~ 560 nm has a good adherence to the substrate. According to the recent report [32], orthorhombic $3\text{WO}_3 \cdot \text{H}_2\text{O}$ actually contains two type of corner-sharing WO_6 octahedras. One type is conducted by a central tungsten atom that is surrounded by six oxygen atoms, while in the second type, two of the oxygen atoms are replaced by a shorter terminal $\text{W}=\text{O}$ bond and longer $\text{W}-(\text{OH})_2$ bond, respectively. Finally, the $3\text{WO}_3 \cdot \text{H}_2\text{O}$ lattice is formed by stacking up layers consisting of these two structural units. Herein, the $\text{CH}_3\text{COONH}_4$ has a capping effect on the stacking of these two structural units, resulting in the formation of nanosticks. Fig. 4 schematically illustrates the formation process of the films grown with and without $\text{CH}_3\text{COONH}_4$.

3.2. Electrochemical and electrochromic properties of the as-prepared $3\text{WO}_3 \cdot \text{H}_2\text{O}$ films

Cyclic voltammograms (CVs) were investigated for both films and shown in Fig. 5(a). These CVs were normalized with respect to the geometric area and to the weight of $3\text{WO}_3 \cdot \text{H}_2\text{O}$ film within that area. During each scan, the films undergo typical reversible color changes from blue to colorless. The recorded current is due to Li^+ intercalation/deintercalation and electron transfer between W^{6+} and W^{5+} according to the following reaction:



The integrated cathodic/anodic current equates to the amount of Li^+ intercalation/deintercalation. It can be clearly seen that the nanostick/nanoparticle film grown with $\text{CH}_3\text{COONH}_4$ shows a higher current density for both intercalation and deintercalation processes over the same time period than the nanobrick one, indicating faster Li^+ intercalation/deintercalation kinetics. The total cathodic charge for the nanostick/nanoparticle film is about $4.2 \text{ mC cm}^{-2} \text{ mg}^{-1}$, compared to only about $2.0 \text{ mC cm}^{-2} \text{ mg}^{-1}$ for nanobrick films.

The CVs of nanostick/nanoparticle and nanobrick films recorded between -1.0 and 1.2 V at various scan speeds are shown in Fig. 5(b) and (c), respectively. It can be seen from Fig. 5(b) that when the scan speed is 5 mV/s , there are two oxidation peaks that appear at about -0.83 and -0.56 V, and two reduction peaks that appear at -0.45 and -0.85 V. With the increased scan speed, the first oxidation peaks disappear, while the second peaks get broader and higher, and the peak positions shift to a higher oxidation potential.

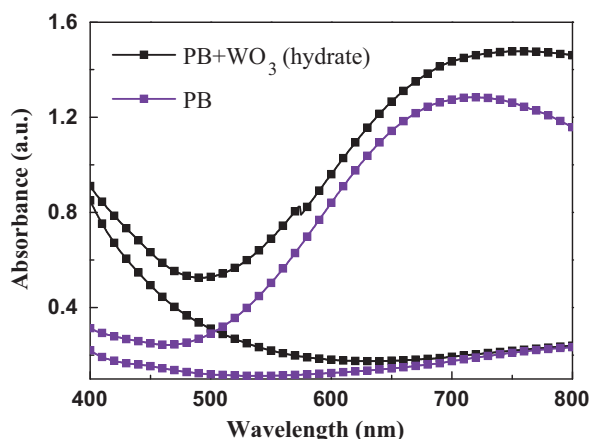


Fig. 7. Optical absorption spectra of a complementary electrochromic device and a single PB layer device at the colored and bleached state under ± 0.8 V, respectively.

The reduction peaks show a similar trend. When the second anodic peak current densities are plotted against the square root of the scan rates, $\nu^{1/2}$, approximately a linear relationship is obtained (inset of Fig. 5(b)), which signifies a diffusion-controlled process [33]. The effective diffusion coefficient D for the diffusing species Li^+ can be estimated from the peak current density (j_p) dependence on the

square root of the potential scan rate ($\nu^{1/2}$) assuming a simple solid state diffusion controlled process [34]:

$$\frac{\delta j_p}{\delta \sqrt{\nu}} = 2.69 \times 10^5 n^3 A C \sqrt{D} \quad (2)$$

$$D = 0.1382 \times 10^{-10} n^{-3} A^{-2} C^{-2} \left(\frac{\delta j_p}{\delta \sqrt{\nu}} \right)^2 \quad (3)$$

where n is the number of electrons transferred in unit reaction, A is the effective geometric surface area of the $3\text{WO}_3 \cdot \text{H}_2\text{O}$ electrode, and C is the concentration of the diffusion species (Li^+). The effective diffusion coefficients D_{Li^+} have been calculated from Eq. (3) to be 2.19×10^{-11} and 1.39×10^{-11} cm^2/s for the intercalation and deintercalation process, respectively, comparable to the reported values [35]. Fig. 5(c) shows the CVs of the nanobrick film recorded at different scan rates, showing a similar profile but smaller current density. The calculated diffusion coefficients D_{Li^+} are 9.60×10^{-12} and 6.101×10^{-12} cm^2/s for the intercalation process and deintercalation process, respectively, which are smaller than those of the nanostick/nanoparticle film. The faster ion diffusion kinetics of the nanostick/nanoparticle film arises from its much rougher surface, which increases its surface area and reduces the ions diffusion path length. The cyclic stability of the nanostick/nanoparticle film was also measured for the 1st, 1000th, and 2000th cycle at room temperature and the results are shown in Fig. 5(d). The current density increases slightly within 2000 cycles, without a clear change in the shape of CV curve, indicating excellent cyclic stability of the film, which is similar to the reported crystalline WO_3 nanoparticles [12]. Chronoamperometry (CA) data were recorded for both films with the potential being stepped from -0.5 V to $+0.5$ V for 40 s, as shown in Fig. 5(e). During each cycle, the $3\text{WO}_3 \cdot \text{H}_2\text{O}$ films change from bleached state to colored state reversibly. For both films, the peak current density of bleaching is much higher than that of coloration, and the current density during bleaching decays faster than coloration. This characteristic is typical for WO_3 with small ion intercalation/deintercalation [20]. The higher bleaching current arises from the good conductivity of tungsten bronze (Li_xWO_3), and the rapid current decay is due to the conductor (Li_xWO_3)-to-semiconductor (WO_3) transition, while the coloring kinetics is always slower than the bleaching one for WO_3 films owing to the higher resistance during WO_3 to Li_xWO_3 transition. Moreover, the peak current densities of coloration/bleaching (-4.9 and 14.1 mA/cm^2) of the nanostick/nanoparticle film are higher than those (-2.4 and 7.5 mA/cm^2) of the nanobrick film. The response time (defined as 70% decrease of current density) for coloration (t_c) and bleaching (t_b) are calculated from current–time transient data from Fig. 5(e). The nanostick/nanoparticle film shows faster coloration/bleaching responses ($t_c \sim 7.0$ s and $t_b \sim 3.0$ s) than those ($t_c \sim 9.0$ s and $t_b \sim 3.5$ s) of the nanobrick film, in well agreement with the results in Fig. 5(a–c). The fast responses for both films are comparable to the spray-pyrolysis deposited amorphous WO_3 film [36].

The *in situ* transmittance responses of the nanostick/nanoparticle and nanobrick film for a 90% transmittance change were also investigated at 754 nm by a ± 0.8 V bias (see Fig. 6(a) and (c)). For the nanostick/nanoparticle film, the coloration time t_c is found to be 7.9 s, and the bleaching time t_b is 4.8 s. However, for the nanobrick film, the coloration time t_c is found to be 7.3 s, and the bleaching time t_b is 7.1 s. The bleaching speed of the nanostick/nanoparticle film is much faster than the nanobrick film, but the coloration speed is a little slower. It is worth to mention that a larger optical modulation of $\sim 45\%$ of the nanostick/nanoparticle film is achieved, compared to that only 38% of the nanobrick film. Coloration efficiency (CE) values of both films were also studied and shown in Fig. 6(b) and (d), respectively. The CE is extracted as the slope of the line fits to the

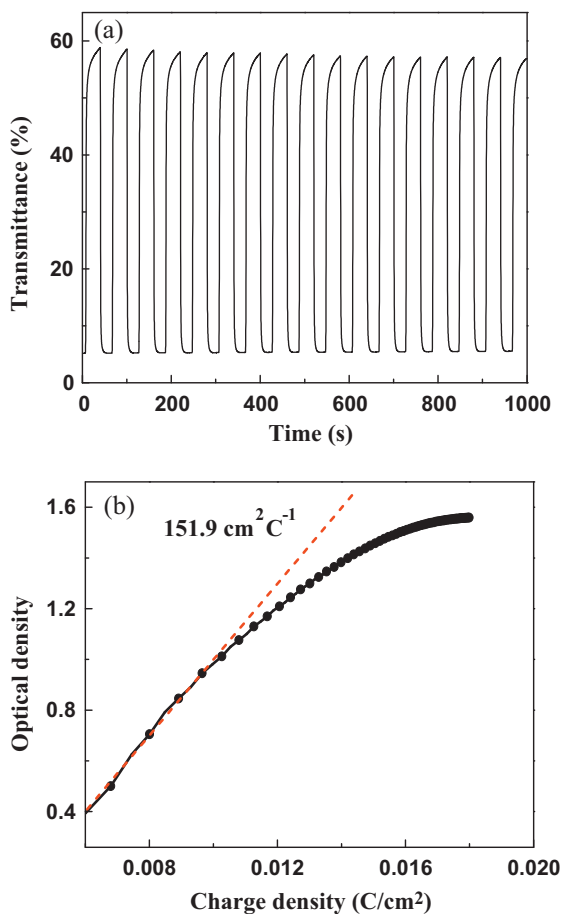


Fig. 8. (a) Switching time characteristics between the colored and bleached states for the complementary electrochromic device measured at ± 0.8 V for 30 s and (b) optical density variation with respect to the charge density recorded at 754 nm.

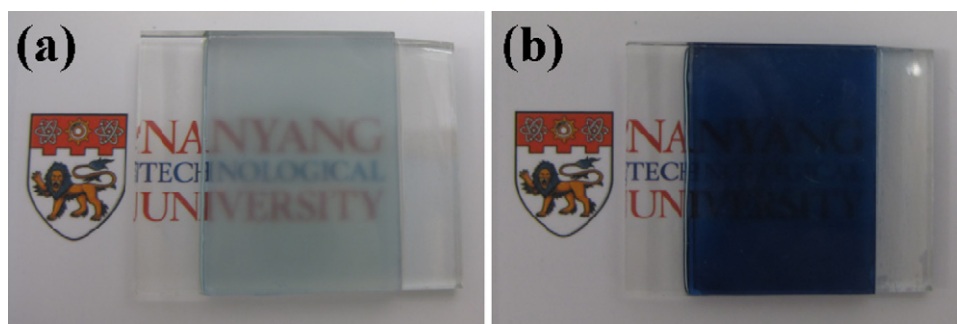


Fig. 9. Photographs of a complementary electrochromic device at the bleached state (a) and (b) the colored state under ± 0.8 V, respectively.

linear region of the curve. It can be seen that the calculated CE of the nanostick/nanoparticle film is $45.5 \text{ cm}^2/\text{C}$, larger than that of the nanobrick film ($36.8 \text{ cm}^2/\text{C}$). The improved electrochromic performance of the nanostick/nanoparticle film is due to its large surface area.

3.3. Optical and electrochromic properties of the complementary device

To further improve the optical contrast, coloration efficiency and switching stability, the nanostick/nanoparticle film is incorporated in an electrochromic device with an anodically colored PB film as a complementary electrochromic layer. The morphology and CV curve of the as-deposited PB film were also investigated and shown in Figs. S1 and S2, respectively (see supplementary information). Fig. 7 shows optical absorption spectra of the complementary electrochromic device and a single PB layer device at the bleached and colored state under a ± 0.8 V bias. Compared with the single PB layer device, the complementary device shows a larger optical modulation above 410 nm, especially in the near IR region, indicating a higher color contrast and larger heat regulation. Moreover, the complementary device depicts a higher absorption in the near UV region at both colored and bleached states due to the absorption of $3\text{WO}_3 \cdot \text{H}_2\text{O}$ films. The above result is highly desired in smart window applications since more heat can be prohibited from entering the interior buildings, resulting in a reduction of cooling loads.

Fig. 8(a) shows the *in situ* coloration/bleaching transmittance response of the complementary device measured at 754 nm. The maximum transmittance modulation (ΔT) of coloration/bleaching was found to be about 54% after applying a ± 0.8 V voltage for 30 s, agreeing well with the absorbance spectra shown in Fig. 7. Obvious color changes can be observed during the switching. The coloration and bleaching time extracted as 90% transmittance changes are found to be 1.3 and 5.7 s, respectively. The switching responses of the complementary device for both the coloration and bleaching processes are much faster than those reported values [30]. For this complementary electrochromic device, limitations of switching response are mainly due to $3\text{WO}_3 \cdot \text{H}_2\text{O}$ electrode. The fast coloration/bleaching kinetics may be attributed to the large active specific area of the rough surface, which facilitates the ions intercalation/deintercalation by reducing their diffusion lengths. CE of the complementary cell was also investigated at its peak absorbance ($\lambda = 754 \text{ nm}$) and shown in Fig. 8(b). The calculated CE value is $151.9 \text{ cm}^2/\text{C}$, comparable to that of the reported WO_3/PB complementary device [30]. And the CE of the complementary device is improved by about 234% compared with a single $3\text{WO}_3 \cdot \text{H}_2\text{O}$ electrochromic layer ($\text{CE} = 45.5 \text{ cm}^2/\text{C}$). Photographs of the complementary device are shown in Fig. 9, depicting a high contrast between the bleached and colored states, which leads to the obvious transparency changes. The

device shows promising applications in energy-saving smart windows.

4. Conclusions

In summary, uniform and well-adhesive $3\text{WO}_3 \cdot \text{H}_2\text{O}$ films consisted of nanosticks/nanoparticles were synthesized via a facile and template-free hydrothermal method by adding $\text{CH}_3\text{COONH}_4$ as the capping agent. Thin films composed of aggregated nanobricks were obtained without $\text{CH}_3\text{COONH}_4$. The nanostick/nanoparticle film depicts faster charge transfer and greater coloration efficiency ($45.5 \text{ cm}^2/\text{C}$) than the nanobrick film ($36.8 \text{ cm}^2/\text{C}$). A complementary electrochromic device based on the nanostick/nanoparticle $3\text{WO}_3 \cdot \text{H}_2\text{O}$ film and PB film was fabricated and demonstrates larger optical contrast (54% at 754 nm), faster switching response ($t_b = 1.3$ s and $t_c = 5.7$ s) and greater coloration efficiency ($151.9 \text{ cm}^2/\text{C}$) than a single $3\text{WO}_3 \cdot \text{H}_2\text{O}$ film device. The complementary device holds great promise for potential applications in energy-saving smart windows.

Acknowledgments

The authors would like to thank the financial support from the Science and Engineering Research Council, Agency for Science, Technology and Research (A*STAR) of Singapore (project Nos. 092 101 0057 and 092 151 0088), Singapore NRF-RF-2009-09, and National Natural Science Foundation of China (NSFC) (project Nos. 61006037 and 61076015).

Appendix A. Supplementary data

Supplementary data associated with this article can be found, in the online version, at doi:10.1016/j.electacta.2011.12.069.

References

- [1] C.G. Granqvist, P.C. Lansaker, N.R. Mlyuka, G.A. Niklasson, E. Avendano, Sol. Energy Mater. Sol. Cells 93 (2009) 2032.
- [2] R.J. Mortimer, Chem. Soc. Rev. 26 (1997) 147.
- [3] C.R. Granqvist, Nat. Mater. 5 (2006) 89.
- [4] C.M. Lampert, Sol. Energy Mater. 11 (1984) 1.
- [5] G.A. Niklasson, C.G. Granqvist, J. Mater. Chem. 17 (2007) 127.
- [6] C.G. Granqvist, A. Azens, A. Hjelm, L. Kullman, G.A. Niklasson, D. Ronnow, M.S. Mattsson, M. Veszelei, G. Vaivars, Sol. Energy 63 (1998) 199.
- [7] R.J. Mortimer, A.L. Dyer, J.R. Reynolds, Displays 27 (2006) 2.
- [8] P. Bonhote, E. Gogniat, F. Campus, L. Walder, M. Gratzel, Displays 20 (1999) 137.
- [9] D.R. Rosseinsky, R.J. Mortimer, Adv. Mater. 13 (2001) 783.
- [10] R. Baetens, B.P. Jelle, A. Gustavsen, Sol. Energy Mater. Sol. Cells 94 (2010) 87.
- [11] C.G. Granqvist, Sol. Energy Mater. Sol. Cells 60 (2000) 201.
- [12] S.H. Lee, R. Deshpande, P.A. Parilla, K.M. Jones, B. To, A.H. Mahan, A.C. Dillon, Adv. Mater. 18 (2006) 763.
- [13] H.D. Zheng, J.Z. Ou, M.S. Strano, R.B. Kaner, A. Mitchell, K. Kalantar-Zadeh, Adv. Funct. Mater. 21 (2011) 2175.
- [14] J.M. O-Rueda de León, D.R. Acosta, U. Pal, L. Castañeda, Electrochim. Acta 56 (2011) 2599.
- [15] S. Hashimoto, H. Matsuoka, J. Electrochem. Soc. 138 (1991) 2403.

- [16] H.G. Choi, Y.H. Jung, D.K. Kim, *J. Am. Ceram. Soc.* 88 (2005) 1684.
- [17] K.Q. Hong, M.H. Xie, H.S. Wu, *Nanotechnology* 17 (2006) 4830.
- [18] D.Z. Guo, K. Yu-Zhang, A. Gloter, G.M. Zhang, Z.Q. Xue, *J. Mater. Res.* 19 (2004) 3665.
- [19] J.M. Wang, E. Khoo, P.S. Lee, J. Ma, *J. Phys. Chem. C* 112 (2008) 14306.
- [20] H. Wang, X. Quan, Y. Zhang, S. Chen, *Nanotechnology* 19 (2008) 065704.
- [21] R.A. Batchelor, M.S. Burdis, J.R. Siddle, *J. Electrochem. Soc.* 143 (1996) 1050.
- [22] S.H. Baeck, K.S. Choi, T.F. Jaramillo, G.D. Stucky, E.W. McFarland, *Adv. Mater.* 15 (2003) 1269.
- [23] S. Balaji, Y. Djaoued, A.S. Albert, R. Bruning, N. Beaudoin, J. Robichaud, *J. Mater. Chem.* 21 (2011) 3940.
- [24] Z.H. Jiao, X.W. Sun, J.M. Wang, L. Ke, H.V. Demir, *J. Phys. D: Appl. Phys.* 43 (2010) 285501.
- [25] J. Zhang, X.L. Wang, X.H. Xia, C.D. Gu, J.P. Tu, *Sol. Energy Mater. Sol. Cells* 95 (2011) 2107.
- [26] Z.J. Gu, T.Y. Zhai, B.F. Gao, X.H. Sheng, Y.B. Wang, H.B. Fu, Y. Ma, J.N. Yao, *J. Phys. Chem. B* 110 (2006) 23829.
- [27] J. Zhang, J.P. Tu, X.H. Xia, X.L. Wang, C.D. Gu, *J. Mater. Chem.* 21 (2011) 5492.
- [28] J. Zhang, J.P. Tu, X.H. Xia, Y. Qiao, Y. Lu, *Sol. Energy Mater. Sol. Cells* 93 (2009) 1840.
- [29] H. Huang, J. Tian, W.K. Zhang, Y.P. Gan, X.Y. Tao, X.H. Xia, J.P. Tu, *Electrochim. Acta* 56 (2011) 4281.
- [30] A. Kraft, M. Rottmann, *Sol. Energy Mater. Sol. Cells* 93 (2009) 2088.
- [31] M. Deepa, T.K. Saxena, D.P. Singh, K.N. Sood, S.A. Agnihotry, *Electrochim. Acta* 51 (2006) 1974.
- [32] L. Zhou, J. Zou, M.M. Yu, P. Lu, J. Wei, Y.Q. Qian, Y.H. Wang, C.Z. Yu, *Cryst. Growth Des.* 8 (2008) 3993.
- [33] A.J. Bard, L.R. Faulkner, *Electrochemical Methods, Fundamentals and Applications*, Wiley, New York, 2001.
- [34] I. Shivanovskaya, M. Hepel, E. Tewksbury, *J. New Mater. Electrochem. Syst.* 3 (2000) 241.
- [35] S.R. Bathe, P.S. Patil, *Smart Mater. Struct.* 18 (2009) 025004.
- [36] S.R. Bathe, P.S. Patil, *Sol. Energy Mater. Sol. Cells* 91 (2007) 1097.